



## Cryogel composites based on hyaluronic acid and halloysite nanotubes as scaffold for tissue engineering

Selin S. Suner<sup>a</sup>, Sahin Demirci<sup>a</sup>, Berkant Yetiskin<sup>c</sup>, Rawil Fakhruллин<sup>d</sup>, Ekaterina Naumenko<sup>d</sup>, Oguz Okay<sup>c</sup>, Ramesh S. Ayyala<sup>b</sup>, Nurettin Sahiner<sup>a,b,\*</sup>

<sup>a</sup> Department of Chemistry & Nanoscience and Technology Research and Application Center, Canakkale Onsekiz Mart University Terzioğlu Campus, 17100 Canakkale, Turkey

<sup>b</sup> Department of Ophthalmology, Morsani College of Medicine, University of South Florida, 12901 Bruce B. Downs Blvd. MDC 21, 33612, Tampa, FL, USA

<sup>c</sup> Department of Chemistry, Istanbul Technical University, 34469 Maslak, Istanbul, Turkey

<sup>d</sup> Bionanotechnology Lab, Kazan Federal University, Kremli uramı 18, Kazan, Republic of Tatarstan 420008, Russian Federation

### ARTICLE INFO

#### Article history:

Received 12 February 2019

Received in revised form 25 February 2019

Accepted 2 March 2019

Available online 03 March 2019

#### Keywords:

Hyaluronic acid  
Halloysite nanotubes  
Composite cryogels  
Tissue engineering  
Blood compatibility

### ABSTRACT

We present here preparation of mechanically strong and biocompatible cryogel composites based on hyaluronic acid (HA) and halloysite nanotubes (HNTs) of various compositions, and their applications as scaffold for different cell growing media. Uniaxial compression tests reveal that the incorporation of HNTs into HA cryogels leads to a ~2.5-fold increase in their Young moduli, e.g., from  $38 \pm 1$  to  $99 \pm 4$  kPa at a HA:HNTs weight ratio of 1:2. Although HA:HNTs based cryogels were found to be blood compatible with  $1.37 \pm 0.11\%$  hemolysis ratio at a HA:HNTs weight ratio of 1:2, they trigger thrombogenic activity with a blood clotting index of  $17.3 \pm 4.8$ . Remarkably, HA:HNTs cryogel composites were found to be excellent scaffold materials in the proliferation of rat mesenchymal stem cells (MSC), human cervical carcinoma cells (HeLa), and human colon cancer cells (HCT116). The cell studies revealed that an increased amount of HNT embedding into HA cryogels leads to an increase of MSC proliferation.

© 2019 Elsevier B.V. All rights reserved.

### 1. Introduction

Hyaluronic acid (HA) or hyaluronan is an anionic non-sulfated glycosaminoglycan (GAG) existing in connective tissues and joints of the human body [1]. HA has many biological functions and can interact with different cells via membrane receptors CD44 (cell surface glycoprotein) performing various tasks such as aggregation, proliferation, cellular stimulation of migration and receptor for HA-mediated motility, and so on [2–6]. HA plays an important biological role in cell development and differentiation in the embryonic period through receptors, maintenance of cellular homeostasis, tissue hydration, regulation of matrix structure and organization of proteoglycan, prevention of intracellular matter migration and arranging cellular movements [1,7]. HA initiates the process of inflammation repair and allows the migration of extracellular matrix cells to the site of inflammation. In the stage of the formation of the granulation tissue and matrix, which is the second stage of wound healing, HA contributes to various cell functions and provides the organization of granulation tissue by forming a hydrated matrix that facilitates cell migration and

interacting with the surface receptors of specific cells. The increased level of HA in the cell proliferation stage after granulation tissue formation facilitates the division of the fibroblasts and that of mitosis. Therefore, it is thought that HA does not directly affect cell proliferation, but indirectly affects mitosis mitogenic activity [8,9]. In an in vitro study to determine the effect of HA on odontoblast and fibroblasts from rat pulp tissue, HA was compared with calcium hydroxide and dentin adhering materials. In the HA-treated cultures, more odontoblast and fibroblast cells were determined in comparison to calcium hydroxide and dentin adhesions indicating that HA possesses great potential in restorative dentin formation. It was shown that HA provides promising conditions in favor of mineralization [10]. Recent evidence also suggests that HA can induce proliferation of human embryonic stem cells (hESCs) and adipose-derived stem cells (ADSC) [11,12]. In addition, it has been reported that HA has a significant effect on the proliferation of human amniotic mesenchymal stem cells (hAMSC) playing an important role in the regulation of proliferation [13].

Halloysite nanotubes (HNTs,  $\text{Al}_2\text{Si}_2\text{O}_5(\text{OH})_4 \cdot n\text{H}_2\text{O}$ ) are two layered natural clay derived from aluminosilicate nanoclay mineral with a hollow nanotubular shape of 10–50 nm in outer diameter, 5–20 nm in inner pore as lumen with a length of 0.5–4  $\mu\text{m}$  [14]. HNTs are environmentally friendly and low-cost materials attracting interest in recent years due to their unique properties such as hydrophilicity, good

\* Corresponding author at: Department of Chemistry & Nanoscience and Technology Research and Application Center, Canakkale Onsekiz Mart University Terzioğlu Campus, 17100 Canakkale, Turkey.

E-mail address: [nsahiner@health.usf.edu](mailto:nsahiner@health.usf.edu) (N. Sahiner).

dispersion ability, biocompatibility, and non-toxicity [15]. HNT/polymer composites possess great potential as wound dressing materials [16], drug delivery vehicles [17], and especially in tissue engineering as scaffold materials [18]. For instance, HNT composites with natural polymers such as chitosan/alginate [19], collagen/chitosan [20], polycaprolactone/gelatin nanofibers [16], chitosan/agarose/gelatin [21], carboxymethylcellulose [22], and hyaluronic acid [23] have been utilized for the reinforcement of tissue engineering scaffolds [24]. It was shown that such composite materials exhibit high thermal and mechanical stabilities, a suitable porous structure and tunable pore sizes as well as chemical surfaces to render good cell attachment and even skin regeneration effects [19].

Cryogels are super porous three-dimensional hydrogel networks which have great advantages in tissue engineering as support materials due to their macroporous, soft, elastic, and sponge-like structures [25–27]. We present here mechanically strong, macroporous HA:HNTs cryogel composites of various compositions exhibiting excellent blood compatibility and biocompatibility suitable as scaffold materials for tissue engineering applications. The composite hydrogels were prepared from aqueous solutions of HA and HNTs in the presence of divinyl sulfone (DVS) as a cross-linker via cryogelation technique at  $-18\text{ }^{\circ}\text{C}$ , i.e., below the freezing temperature of the reaction system. Cross-linking reactions thus proceed in the unfrozen domains of the apparently frozen system whereas ice crystals present in the gelation system act as a template to form pores. As will be seen below, increasing HNT content of the cryogels up to a HA:HNTs weight ratio of 1/2 significantly improves their mechanical and thermal behavior and simultaneously, promotes cell adhesion, cell growing/proliferation, and migration of different types of cells to be used as potential cell growing scaffolds. To highlight the biomaterial nature of the present composite cryogels, their blood compatibility via hemolysis and blood clotting tests, the capability as scaffold by means of growing of rat mesenchymal stem cells, human cervical carcinoma cells (HeLa) and human colon cancer cells (HCT116) and their effects on the mitochondrial enzyme activity were also investigated using MTT and Resazurin assays.

## 2. Materials and methods

### 2.1. Materials

Hyaluronic acid sodium salt obtained from *Streptococcus equi* (HA, 91%, Alfa Aesar,  $M_w = 1\text{ MDa}$ ), halloysite nanoclay particles of 30–70 nm in diameter and 1–3  $\mu\text{m}$  in length (Sigma-Aldrich), divinyl sulfone (DVS, 96%, Merck), calcium chloride anhydrous (99%, Aldrich) and sodium chloride (for analysis ACS, ISO, Reag. Ph Eur, Merck) were used as received. Ultra-pure distilled (DI) water (18.2 M $\Omega$  cm, Millipore-Direct Q UV3) was used in the preparation of all the relevant solutions.

### 2.2. Preparation HA cryogels with and without HNTs

Macroporous HA cryogels without HNTs were prepared according to a method reported earlier with some modifications [23]. HA solution was first prepared at 0.035 g/mL concentration in 0.2 M NaOH and then kept at  $-18\text{ }^{\circ}\text{C}$  for 2 min. After addition of 10 mol% DVS with respect to the HA repeating unit at 1000 rpm, the solution was immediately placed into plastic pipettes of 8 mm in diameter to conduct cryogelation gelation in a freezer at  $-18\text{ }^{\circ}\text{C}$  for 24 h. The prepared HA cryogels were then removed from the pipettes and cut into specimens of about 10 mm in length. The gel specimens were washed with excess DI water for several times to remove off unreacted chemicals. Water swollen HA gel specimens were dried in a freeze-drier for 72 h, and finally stored in sealed containers until use.

For the preparation of composite cryogels with HA:HNTs weight ratios of 1:0.5, 1:1, and 1:2, HNTs weighing 0.0525, 0.105, and 0.210 g, respectively, were dispersed separately in 1 mL of aqueous 0.2 M NaOH solution under sonication for 10 min. The solutions were mixed with

3 mL of 0.2 M NaOH solution of HA (0.035 g/mL) for 2 h at 300 rpm mixing rate, and then cooled to  $-18\text{ }^{\circ}\text{C}$  for 2 min. After addition of 10 mol% DVS, the cryogelation reactions were carried out at  $-18\text{ }^{\circ}\text{C}$  as described above.

### 2.3. Characterization

The visualization of HNTs was acquired via TEM imaging (JEOL JEM-1220) operating at 80 kV. For this purpose, HNTs were suspended in ethanol and a drop of this suspension was placed on the grid and dried at room temperature, before imaging.

Scanning electron microscopy (SEM) images of HA and HA:HNTs cryogels were obtained using a Jeol JSM-5600 LV SEM instrument operating at 10 kV voltage. The freeze-dried cryogel specimens were placed onto a carbon tape attached SEM stub and coated with gold to a few nm thickness for SEM imaging.

Fourier transform infrared (FT-IR) spectra of HA and HA:HNT cryogels were taken on a Nicolet iS10 spectrometer (Thermo Scientific, Waltham, MA, USA) between 650 and 2000  $\text{cm}^{-1}$  range by employing attenuated total reflectance (ATR) with 4  $\text{cm}^{-1}$  resolutions.

The thermogravimetric analysis (TGA, SII 6300 TG/DTA, Exstar) of the cryogels was conducted under  $\text{N}_2$  atmosphere at a flow rate of 200 mL/min by heating the gel specimens up to 1000  $^{\circ}\text{C}$  with 10  $^{\circ}\text{C}/\text{min}$  heating rate.

Uniaxial compression tests were carried out on cryogel specimens both in equilibrium swollen and dried states. The specimens in cylindrical shapes with a diameter of 8 mm were cut into small pieces of about 3 mm in length. The compression tests were performed at room temperature ( $23 \pm 2\text{ }^{\circ}\text{C}$ ) on a Zwick Roell test machine using a 500 N load cell at a constant crosshead speed of 10 mm/min. A pre-load of 0.01 N was applied to ensure a complete contact between the sample and the surface. Young's modulus  $E$  of the cryogels was calculated from the slope of the stress-strain curves between 5 and 15% compressions. Compressive stress was given by its nominal  $\sigma_{nom}$  and true values  $\sigma_{true}$ , which are the forces per cross-sectional area of the undeformed and deformed specimen, respectively. Assuming constancy of the gel volume during compression, the true stress is related to the nominal stress by  $\sigma_{true} = \sigma_{nom} \lambda$ , where  $\lambda$  is the deformation ratio. The strain was given by fractional deformation  $\varepsilon$ , i.e.,  $\varepsilon = 1 - \lambda$ .

### 2.4. Blood compatibility

Hemolysis and blood clotting tests were used to determine the blood compatibility of composite cryogels with HA:HNTs weight ratios of 1:0, 1:0.5, 1:1, and 1:2 using a similar procedure reported before [28]. Fresh blood samples were gathered from healthy volunteers and placed into EDTA containing hemogram tubes in accordance with the Human Research Ethics Committee of Canakkale Onsekiz Mart University (KAEK-2016-27).

In hemolysis method, 1 mL of the blood was diluted with 1.25 mL of 0.9% NaCl solution, preheated at 37.5  $^{\circ}\text{C}$ . HA:HNTs based cryogel specimens weighing 10 mg were placed into 10 mL of 0.9% NaCl solution at 37.5  $^{\circ}\text{C}$ . Then, 0.2 mL of diluted blood was slowly added to this cryogel containing solution and incubated at 37.5  $^{\circ}\text{C}$  in a shaker. After 1 h, the cryogel containing blood solution was centrifuged at 100 g for 5 min and the released amount of hemoglobin through hemolysis of erythrocyte cells was measured via the absorbance of the supernatant blood solution with UV-Vis spectrophotometer at 542 nm. The hemolysis ratio % of the HA:HNTs based cryogels was calculated by the following equation:

$$\text{Hemolysis ratio}\% = (A_{\text{cryogel}} - A_{\text{negative}}) / (A_{\text{positive}} - A_{\text{negative}}) \times 100 \quad (1)$$

where  $A_{\text{cryogel}}$  is the absorbance value of the HA:HNTs based cryogel containing blood solution,  $A_{\text{negative}}$  is the negative control as the absorbance value of 0.2 mL of diluted blood in 0.9% NaCl solution, and  $A_{\text{positive}}$

is the positive control as the absorbance value of 0.2 mL of diluted blood in 10 mL of DI water. Each value was averaged from four parallel measurements.

To determine the blood clotting capacity of HA:HNTs cryogels, 64.8 mL of 0.2 M  $\text{CaCl}_2$  solution was added to 0.81 mL of fresh blood.

Then, the cryogel specimen weighing 10 mg was swollen with 100  $\mu\text{L}$  of 0.9% NaCl solution, and 0.27 mL of  $\text{CaCl}_2$  containing blood solution was dropped on cryogel network. This blood interacted cryogel piece was incubated at 37.5  $^\circ\text{C}$  in a shaker. After 10 min, 10 mL of DI water was immediately placed onto this blood containing cryogel and

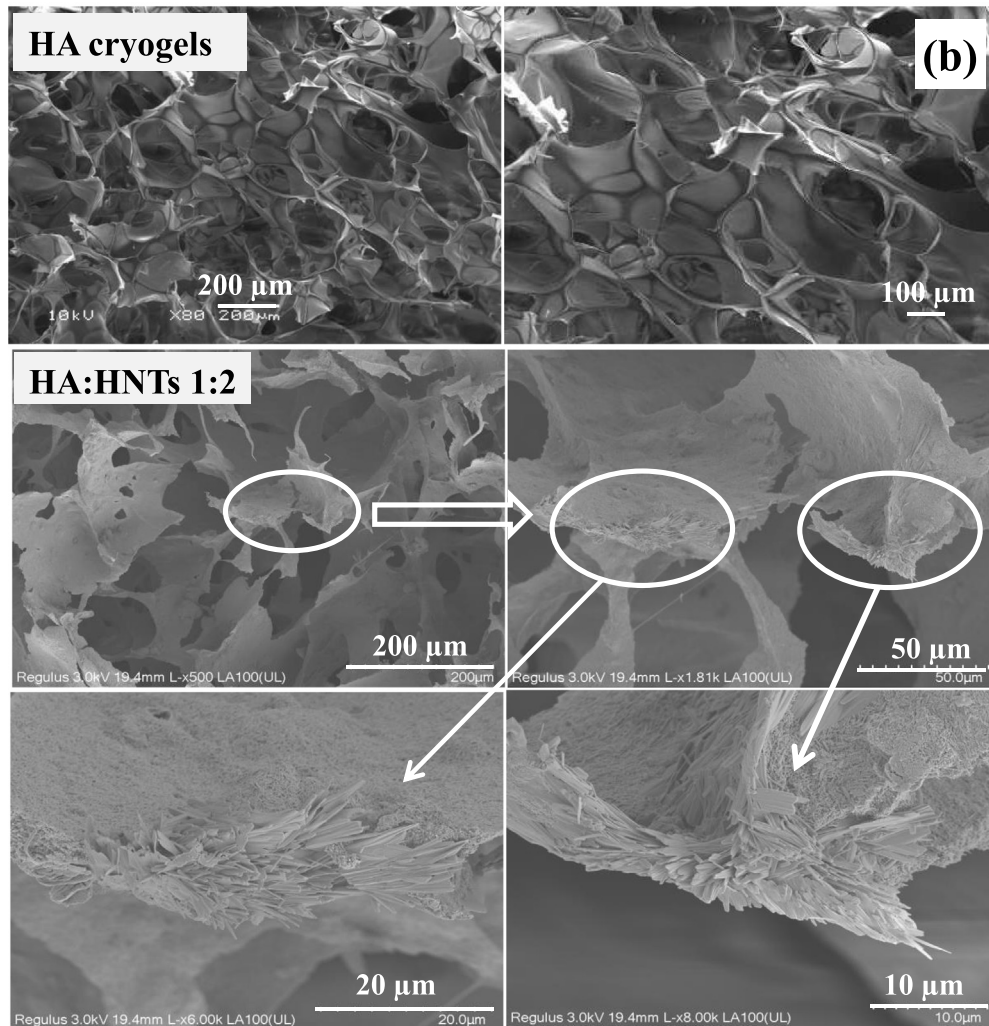
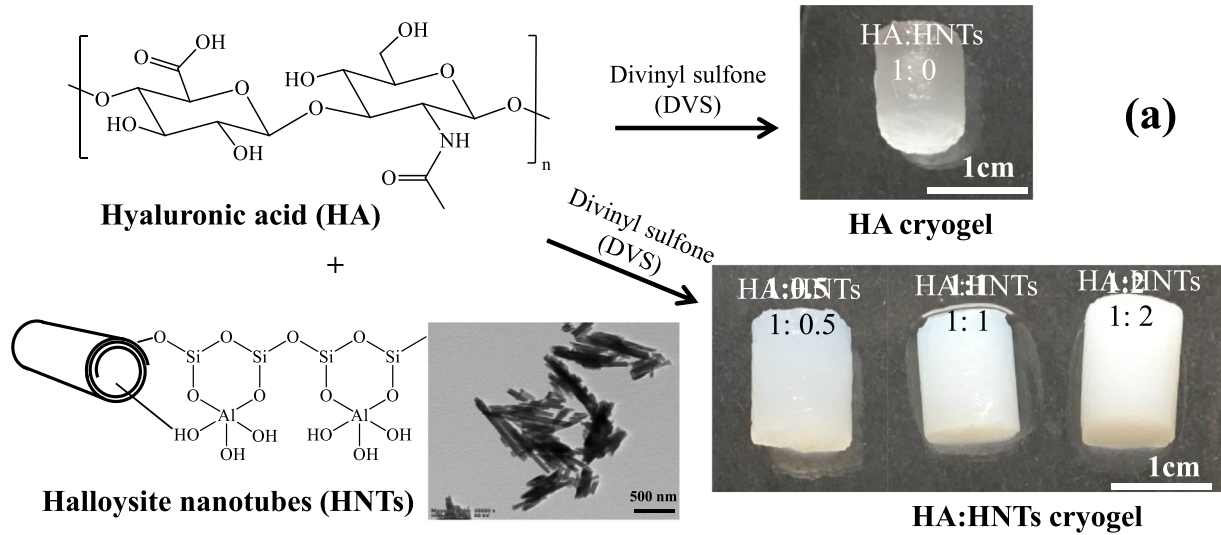


**Fig. 1.** (a) Schematic illustration of bare HA and HA:HNTs composite cryogels at various HNTs ratios such as 1:0, 1:0.5, 1:1, and 1:2, and TEM images of HNTs and digital camera images of swollen cryogels. (b) SEM images of the cryogels at HA:HNTs weight ratios of 1:0 and 1:2 where white arrows clearly show the presence of HNT within the HA matrix.

centrifuged at 100 g for 30 s. The supernatant blood solution was diluted with 40 mL of DI water and incubated for 1 h at 37.5 °C in a shaker. The non-coagulating blood amount was determined by the absorbance of the supernatant solution using UV-Vis spectrophotometer at 542 nm. The blood clotting indexes of the HA:HNTs based cryogels were calculated by using Eq. (2):

$$\text{Blood clotting index} = (A_{\text{cryogel+blood}}/A_{\text{blood}}) \times 100 \quad (2)$$

where  $A_{\text{cryogel+blood}}$  is the absorbance of the non-coagulating blood solution which contacting with the cryogels,  $A_{\text{blood}}$  is the absorbance of 0.25 mL fresh blood diluted with 50 mL DI water. Each value was averaged from four parallel measurements.

For statistical analysis, *t*-tests were used to determine whether the hemolysis and blood clotting tests in the presence of HA:HNTs based cryogels were significantly different from the HA cryogel. The data were expressed as  $*p < 0.05$ , versus HA cryogel.

## 2.5. Cell cultures

Mammal cell cultures (rat mesenchymal stem cells (MSC), human cervical carcinoma cells (HeLa) and human colon cancer cells

(HCT116)) were obtained from American Type Culture Collection (ATCC). MSC and HeLa cells were cultivated in Minimum Essential Medium Eagle - alpha modification ( $\alpha$ MEM) (PAA laboratories) supplemented with 10% of fetal bovine serum (FBS) (PAA laboratories), 0.1% penicillin ( $10 \text{ U mL}^{-1}$ )/streptomycin ( $10 \mu\text{g mL}^{-1}$ ). HCT116 cells were cultured in Dulbecco's Modified Eagle's Medium (DMEM) supplemented with 10% of FBS, 0.1% penicillin ( $10 \text{ U mL}^{-1}$ )/streptomycin ( $10 \mu\text{g mL}^{-1}$ ). All cell cultures were incubated under a humidified atmosphere with 5%  $\text{CO}_2$  at 37 °C.

### 2.5.1. Cells proliferation on scaffolds

Scaffolds with a diameter of 10 mm were cut into slices with a thickness of about 0.5–0.7 mm, placed into 48-wells culture plates and sterilized using UV irradiation for 2 h for both sides. Then slices were mounted into appropriate growth medium and placed into  $\text{CO}_2$  incubator (5%  $\text{CO}_2$ , 37 °C) for 30 min for equilibration of conditions. First, the growth media were aspirated, then the cells were seeded on scaffolds ( $2 \times 10^6$  cells per slice) in 50  $\mu\text{L}$  of growth media and incubated for 24 h. Then the scaffolds colonized by cells were washed with saline buffer, fixed with 4% paraformaldehyde for 20 min, washed again and stained with DAPI to visualize the nuclei and fluorescein to stain scaffold polymer material. Images were obtained using Confocal Laser Scanning

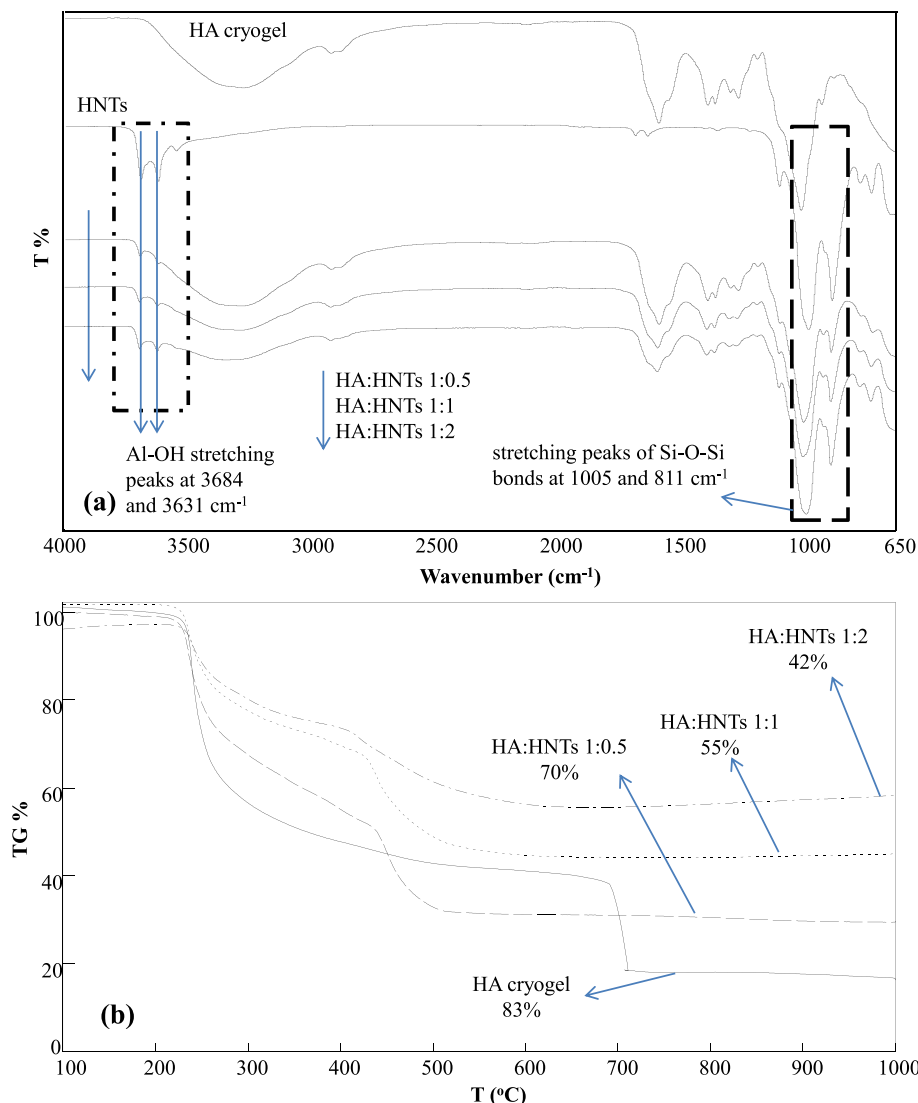


Fig. 2. (a) FT-IR spectrum, and (b) TGA thermograms of bare HA and HA/HNTs cryogel composites of various weight ratios indicated.

Microscope (CLSM) Carl Zeiss LSM 780 equipped with planapochromat 40× and 63× oil immersion objectives and laser excitation in UV (405/410–508 nm) and green (488/490–606 nm) channels. The images obtained were processed using ZEN 9.0 software (Carl Zeiss AG).

### 2.5.2. Qualitative MTT assay

A qualitative in situ viability assay of HeLa, HCT116 and MSC cells grown on scaffolds was performed by incubation of scaffolds with cells in 2 mL of DMEM and 200  $\mu$ L of MTT (dimethylthiazoldiphenyltetrazolium bromide) solution (5 mg/mL; Sigma-Aldrich) per well for 4 h at 37 °C under a humidified atmosphere with 5% CO<sub>2</sub>. Dark purple color indicated the activity of mitochondrial enzymes of cells. Images were captured using a color digital camera.

### 2.5.3. Resazurin reduction assay

Cell viability was also assessed using resazurin reduction test, which estimates the mitochondrial dehydrogenases activity of live cells. Scaffolds inoculated with cells were incubated for 48 h in culture medium at 37 °C in humidified atmosphere with 5% CO<sub>2</sub>. Then, the culture medium was replaced with resazurin solution (0.01 mg/mL) in the culture medium and the plates were incubated for 24 h. 200  $\mu$ L of the reaction media from each experimental well were transferred to the 96-well plates, and the color density of resorufin was measured using a microplate spectrophotometer (Thermo Fisher Multiskan) at 595/570 nm. Resazurin reduction rate is directly proportional to the number of viable cells. Experimental data were expressed as the mean  $\pm$  standard deviation (SD) for  $n = 3$ .

## 3. Results and discussion

HA:HNTs cryogel composites with various compositions were prepared by cryogelation at  $-18$  °C in the presence of DVS as a cross-linker and their potential applicability as a cell growing scaffold were investigated. For comparison, HA cryogels without HNTs were also prepared under identical conditions. The vinyl groups of DVS are known to attack the hydroxyl groups of HA leading to the formation of a 3D network of HA molecules as illustrated in Fig. 1a.

Conducting the cross-linking reactions under a cryogenic condition provided cryoconcentration of the reactants in the unfrozen domains whereas frozen domains acted as a template for the formation of pores. Fig. 1a shows TEM images of the HNTs used in the preparation of cryogel composites. They are 0.5–4  $\mu$ m in length and nearly 100 nm in inner diameter with tubular shapes containing positively charged alumina inner lumen and negatively charged silicate outer surfaces. Optical images of water-swollen gel specimens reveal that pure HA cryogels are almost transparent whereas HA:HNTs cryogel composites are opaque and opacity increases as the amount of HNTs is increased (Fig. 1a). Fig. 1b showing SEM images of pure HA and HA:HNTs cryogels demonstrate that they all are macroporous with pores between 50 and 500  $\mu$ m in diameter. As compared to the bare HA cryogels exhibiting a smooth surface of the pore walls, HA:HNTs cryogel composites possess rough surfaces and the roughness increases with increasing amount of HNTs within the cryogel structure. The formation of smooth and rough pore surfaces without and with HNTs, respectively, is due to the accumulation of the nanotubes on the pore walls, which are visualized in Fig. 1b (indicated by the arrows).

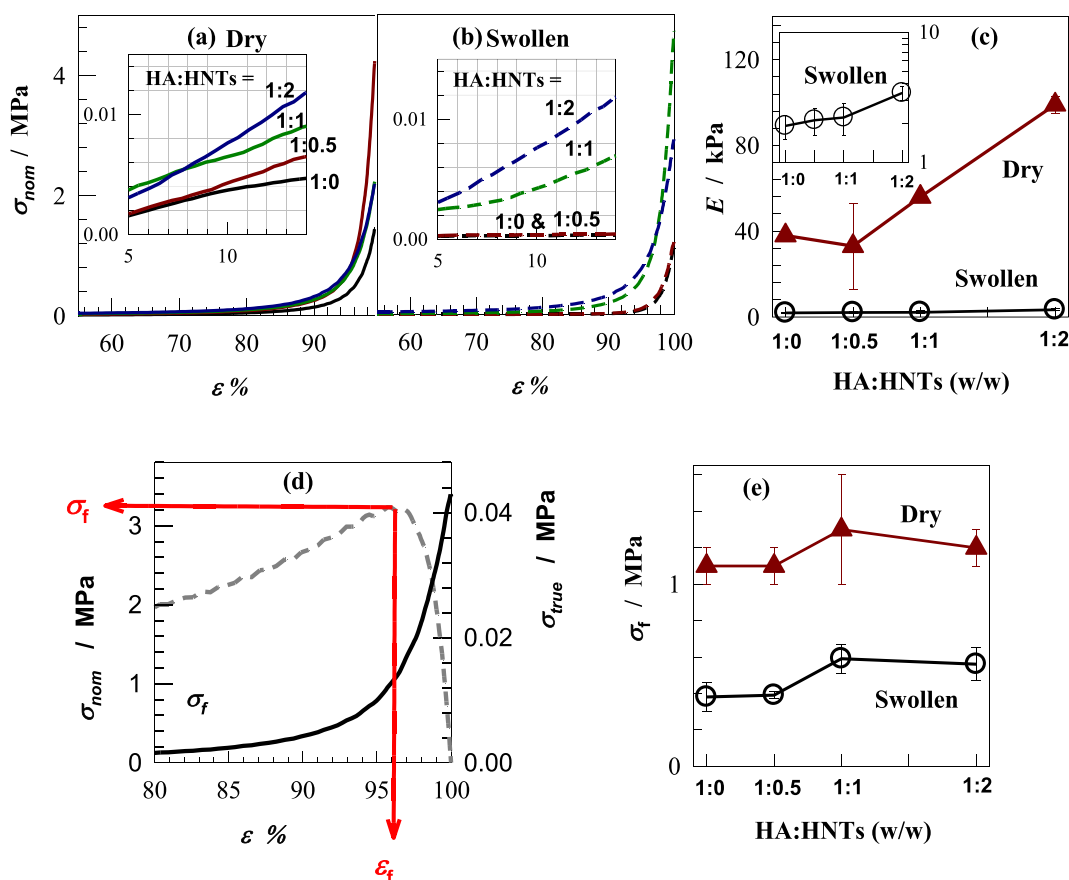


**Fig. 3.** Compressive stress-strain curves of (a) dry and (b) swollen cryogels with various HA:HNTs weight ratios as indicated. The nominal stress  $\sigma_{nom}$  was plotted against the strain  $\epsilon$ . The insets to the figures present the same curves between 5 and 15% strains. (c): Young's moduli  $E$  of dry and swollen cryogels plotted against their HA:HNTs weight ratios. The inset shows a zoom-in between 1 and 10 kPa in logarithmic scale (d): Typical  $\sigma_{nom} - \epsilon$  (solid curve) and  $\sigma_{true} - \epsilon$  curves (dashed curve) of cryogels. The red lines present the calculation of the fracture stress  $\sigma_f$  from the maximum in  $\sigma_{true} - \epsilon$  curve. (e): Fracture stress  $\sigma_f$  of the cryogels shown as a function of their HA:HNTs weight ratios.

To confirm the incorporation of HNTs within the cryogel network, the gel specimens were subjected to FT-IR measurements. Fig. 2a shows typical FT-IR spectra of HA cryogels, HNTs, and HA:HNTs cryogel composites at various compositions. HA cryogel exhibits three main peaks at 3300–3100, 1611, and 1041  $\text{cm}^{-1}$ , corresponding to —OH stretching, carboxylate groups, and S=O stretching from the cross-linker (DVS) units, respectively. The spectrum of HNTs exhibits Al-OH stretching peaks at 3684 and 3631  $\text{cm}^{-1}$ , bending peaks for Al-OH bonds at 918  $\text{cm}^{-1}$ , and the stretching of Si—O—Si bonds at 1005 and 811  $\text{cm}^{-1}$ . Moreover, HA:HNTs cryogel composites formed at various compositions exhibit typical FT-IR peaks of their components, e.g., stretching of carboxylate groups at 1618  $\text{cm}^{-1}$ , Al—OH stretching peaks at 3686 and 3633  $\text{cm}^{-1}$ , and Si—O—Si bonds at 1009  $\text{cm}^{-1}$ , with small shifts in peak positions due to interaction of filling materials with HA matrix.

The thermal behavior of the cryogels was investigated by TGA measurements. Fig. 2b compares the thermal stability of HA and HA:HNTs cryogels using their TGA thermograms. Both HA cryogel and its composites start to degrade at around 220–230 °C and the degradation continues up to around 270–280 °C. The weight losses after this first degradation step are 39, 27, 18, and 16% for bare HA and HA composites with 1:0.5, 1:1, and 1:2 weight ratios, respectively. Moreover, 2nd degradation step of bare HA cryogel appears between 690 and 710 °C with a weight loss of 82% that increases to 83% upon heating to 1000 °C. In contrast, for HA:HNTs composites at 1:0.5, 1:1, and 1:2 weight ratios, the weight losses observed between 420 and 510 °C are 68, 52, and 40%, that increase to 70, 55 and 42% when heated to 1000 °C, respectively. The results thus show that increasing amount of HNTs in HA cryogels results in a decrease in their weight losses at 1000 °C from 83 to 42%, revealing increasing thermal stability of HA cryogels.

Fig. 3a and b show compressive stress-strain curves of dry and swollen cryogels, respectively, prepared at various HA/HNTs weight ratios.

The insets to the figures present the initial linear portions of the same curves between 5 and 15% strains, which were used for the calculation of Young's moduli  $E$  of the cryogels (Fig. 3c). The results reveal an enhancement in the mechanical properties of the cryogels as the HNTs content is increased. For instance, in the absence of HNTs, that is, for the dried pure HA cryogel, Young's modulus  $E$  is  $38 \pm 1$  kPa whereas it increases with increasing HNTs content and becomes  $99 \pm 4$  kPa at a HA:HNTs weight ratio of 1/2. As expected, the moduli  $E$  of swollen cryogels are smaller than those of dried ones and they slightly increase from  $1.9 \pm 0.4$  to  $3.4 \pm 0.4$  kPa with increasing HNTs content.

Fig. 3a and b also show that both dried and swollen cryogels can completely be compressed and they sustain up to about 4 MPa nominal stresses. However, converting the nominal stress ( $\sigma_{nom}$ ) to its true value ( $\sigma_{true}$ ) and plotting  $\sigma_{true}$  against the strain  $\varepsilon$  result in stress-strain curves exhibiting maxima at lower compressions as can be seen in Fig. 3d. This means the occurrence of a microscopic crack in the cryogels that cannot be detected from  $\sigma_{nom} - \varepsilon$  curves [29]. Therefore, the fracture stresses  $\sigma_f$  of the cryogels were determined from the maxima of  $\sigma_{true} - \varepsilon$  curves and they are plotted against the HA:HNTs ratio in Fig. 3e. It is seen that the fracture stress  $\sigma_f$  of the cryogels does not change much with their HNTs contents and remains at around 1.2 and 0.6 MPa for dry and swollen cryogel specimens, respectively. The results thus indicate that the modulus, i.e., cross-link density of the cryogels significantly increases with the amount of HNTs whereas fracture stress remains unaffected.

Materials such as cryogels as potential tissue scaffolds that will be in contact with blood, in vivo applications needed to be tested for their effect on blood cells and thrombogenic activity that may have paramount significance in the vascularization of tissues and organs. As cryogel based materials have been known for many biomedical applications including vivo tissue engineering, wound dressing and even generation of blood vessel and so on [3,9–13,31], the blood compatibility tests of such materials need to be tested. Therefore, the

blood compatibility of bare HA cryogels and composites at various HA:HNTs weight ratios were investigated using hemolysis and blood clotting tests as demonstrated in Fig. 4. Hemolysis is the destruction of erythrocyte cells and for any blood contacting material with a hemolysis ratio of up to 5% can be considered as a blood compatible material [30]. The results in Fig. 4a show that all cryogels reported here are non-hemolytic materials with hemolysis ratios increasing from  $0.63 \pm 0.38$  to  $1.37 \pm 0.11\%$  as the HA:HNTs weight ratio is increased from 1:0 to 1:2. Thus, the hemolysis ratio is a slightly increasing function of HNTs content of the cryogels, yet it remains much below its critical value indicating that they all have good blood compatibility and no statistically significant results were observed for HA:HNTs cryogels in comparison with HA cryogels ( $*p < 0.05$ ).

Another important test for blood contacting materials is blood clotting tests which indicate the antithrombogenic activity of the materials upon contact with the blood. Fig. 4b presenting blood clotting indices of the cryogels reveals that all the cryogels have similar clotting indices, i.e.,  $16 \pm 1$ . These results thus show that both HA and composite cryogels have similar thrombogenic properties that can trigger the clotting of the blood on the occasion of contacting with the blood. Therefore, the materials can be used in the hemostatic treatment in the biomedical applications. According to the statistical analysis of blood clotting tests, only cryogels prepared at a HA:HNTs weight ratio of 1:2 were significantly different ( $p < 0.05$ ) with HA cryogels.

Confocal laser scanning microscopy images in Fig. 5 show the growth of rat mesenchymal stem cells (rat MSC) on composite HA scaffolds. The cryogel specimen with a HA:HNTs weight ratio of 1:0 showed relatively weak adhesive properties because cells formed rarely clusters inside the compartments of porous material. Proliferation of cells was observed inside the compartments, i.e., within the pores of the scaffold, and the cells were aggregated into compact spheroids. As discussed above, an increasing amount of HNTs in composite scaffolds resulted in improved mechanical properties. Simultaneously, within

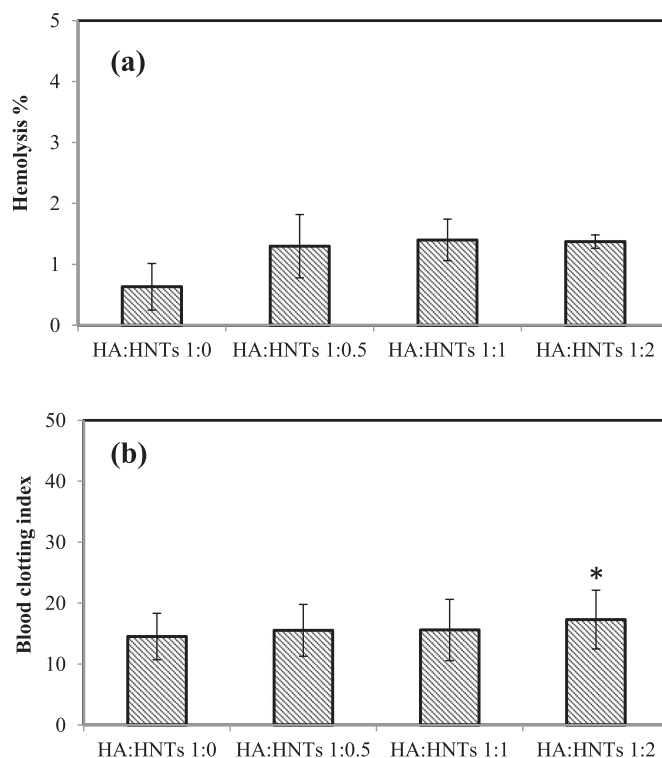
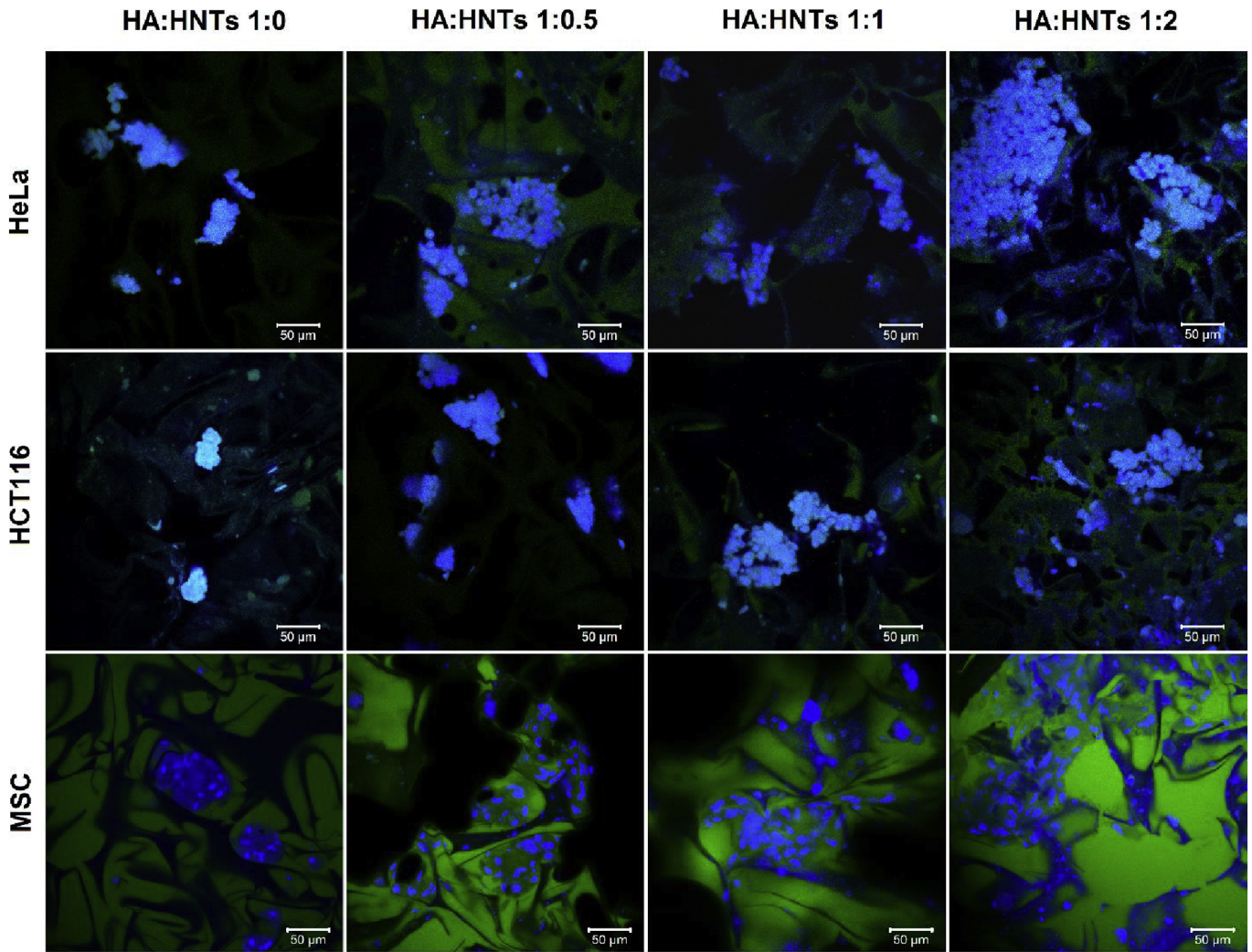


Fig. 4. (a) Hemolysis and (b) blood clotting indices of bare HA and HA:HNTs composite cryogels. Statistical analyses were evaluated by  $t$ -test and no significantly different results were observed for HA cryogels and HA:HNTs composites. The data were expressed as  $*p < 0.05$ , versus HA cryogel.



**Fig. 5.** The growth of rat mesenchymal stem cells (rat MSC) on composite scaffolds with various HA:HNTs weight ratios indicated. Nuclei of cells were stained with DAPI (blue) whereas scaffold material was tinted with fluorescein diacetate (FDA) (green).

the scaffolds prepared at high HNTs contents such as those with HA:HNTs weight ratios of 1:1 and 1:2, cells distributed outside the limits of pores and widely spread on the whole scaffold surfaces as illustrated in Fig. 5.

Halloysite nanotubes are recognized as a versatile material for industrially relevant functional polymeric composites and considered as a promising material for alteration of tissue engineering materials properties [31]. One of the advantages that make halloysite promising filler for biopolymer materials is the formation of stable dispersions in water and redispersion after sedimentation [32]. Tubular clay nanoparticles can be easily loaded with different compounds, such as drugs, growth and proliferation factors for the fabrication of 'functional tissue scaffold' [33].

To demonstrate the viability, proliferation, and distribution of different cell lines on the scaffolds we performed a slightly modified in situ MTT test [21]. This method commonly based on measuring the optical density of the purple formazan formed inside live and metabolically active cells as a result of MTT reduction [34]. Here, we used the qualitative visualization based on the incubation of scaffolds with cells in MTT solution in cell culture plates as shown in Fig. 6. After incubation, the formazan crystals had been formed by living cells grown on scaffolds yielding dark purple color. In the case of cell-free scaffolds, they remain colorless.

We also have used the resazurin assay to demonstrate the viability of cells growing on HA scaffolds e.g., pure HA or HA with halloysite as

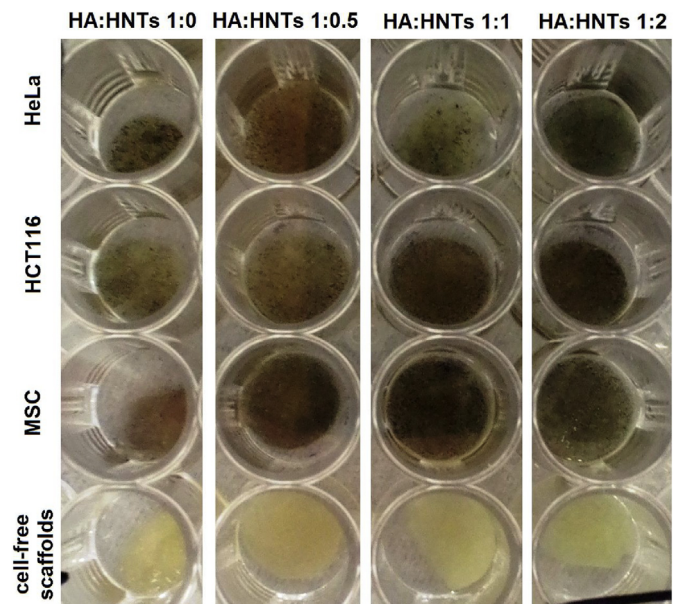


**Fig. 6.** Qualitative MTT assay results of HeLa, HCT116 and MSC in growth medium seeded on composite scaffolds with various HA:HNTs weight ratios indicated. Dark purple staining indicates the metabolic active cells distribution onto scaffolds.

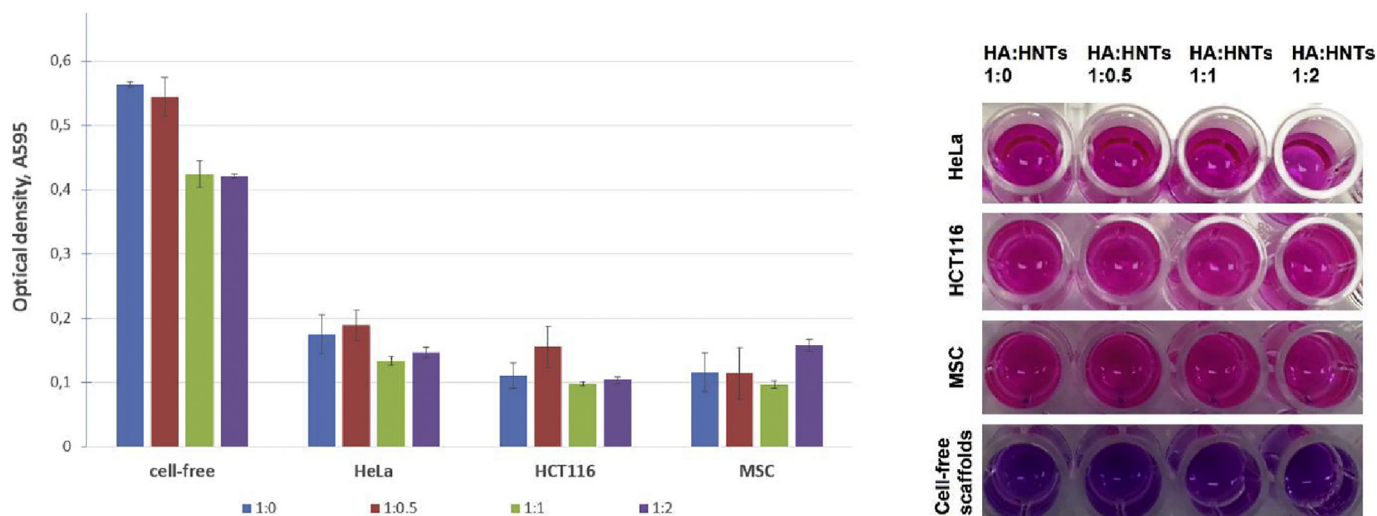


**Fig. 7.** Resazurin assay data demonstrating the influence of different scaffold compositions on mitochondrial enzyme activity. Pink color indicates the viable cells with high level of cells enzymatic activity. Numbers in diagram legend indicate the ratio of HA:HNTs.

demonstrated in Fig. 7. This method allows confirming the spreading and metabolic activity of cells on the scaffolds. The test is based on the enzymatic activity of mitochondria reducing the blue dye resazurin to the pink dye resorufin. The resazurin assay demonstrated the viability of cells grown on different types of scaffolds. The cells were seeded on the top of the scaffold discs. After 24 h discs were transferred into new plates to avoid estimation of cells grown on the bottom of wells. Incubation of scaffolds in the presence of resazurin dye led to the change of blue color to pink due to the enzymatic activity on the HA/HNTs scaffolds discs.

According to the recent publications, halloysite is biocompatible for a wide range of microbial, cell culture and animal models. The range of safe concentrations of clay nanotubes reaches 0.2 mg/mL, making it one of the safest inorganic fillers [35]; the safe concentrations for freshwater protist *Paramecium caudatum* were up to 10 mg/mL [36]. Previously we reported that even the addition of tubes in a volume of 3–6% led to an improvement in mechanical properties and did not reduce biocompatibility [21]. Addition of a relatively large amount of nanotubes e.g., up to 50% into the biopolymeric matrix in the present study did not lead to any inhibiting effects on the growth and proliferation of cells and has led to the improved cellular adhesion and subsequent substrate colonization.

#### 4. Conclusions

Superporous HA:HNTs cryogel composites were successfully prepared at different HA:HNTs weight ratios e.g., 1:0, 1:0.5, 1:1, and 1:2 under cryogenic condition. SEM images disclose that cryogel composites are highly porous with superporous structure with pore sizes ranging from 50  $\mu\text{m}$  to 500  $\mu\text{m}$ . The thermal and mechanical stabilities were found to increase with increasing content of the HNTs inside the composite structure. Bare HA and HA:HNTs cryogel composites were found to be non-hemolytic materials in the range of 0.63 to 1.39% hemolysis ratios, and they were found slightly hemostatic with 14.5–17.3 blood clotting indexes upon contacting with the human blood. Furthermore, HNTs on the cryogel scaffolds showed improved viability, proliferation, adhesion and the growth of the different types of cell lines such as mesenchymal stem cells (MSC), cervical carcinoma cells (HeLa) and colon cancer cells (HCT116). Therefore, the prepared HA:HNTs cryogel composites are promising materials as tissue engineering scaffolds with their macroporous structure, high thermal and mechanical stability, good blood compatibility. The extraordinary properties of the cryogel composites presented here can find many applications in

the biomedical field in promoting of the cell viability, cell proliferation, and adhesion effects.

#### Acknowledgment

The work was performed within the Russian Government Program of Competitive Growth of Kazan Federal University. It was funded by RFBR grant 18-29-11031-mk and by the subsidy allocated to Kazan Federal University for the state assignment in scientific activities (#16.2822.2017/4.6).

#### References

- [1] J. Necas, L. Bartosikova, P. Brauner, J. Kolar, Hyaluronic acid (hyaluronan): a review, *Vet. Med. Czech.* 53 (2008) 397–411.
- [2] L. Bourguignon, D. Zhu, H. Zhu, CD44 isoform-cytoskeleton interaction in oncogenic signaling and tumor progression, *Front. Biosci.* 3 (1998) 637–649.
- [3] V.B. Lokeshwar, N. Iida, L.Y. Bourguignon, The cell adhesion molecule, GP116, is a new CD44 variant (ex14/v10) involved in hyaluronic acid binding and endothelial cell proliferation, *J. Biol. Chem.* 271 (1996) 23853–23864.
- [4] G. Christofori, Changing neighbors, changing behavior: cell adhesion molecule-mediated signaling during tumor progression, *EMBO J.* 22 (2003) 2318–2323.
- [5] E.A. Turley, P.W. Noble, L.Y. Bourguignon, Signaling properties of hyaluronan receptors, *J. Biol. Chem.* 277 (2002) 4589–4592.
- [6] K. Kouvidi, A. Berdiaki, M. Tzardi, E. Karousou, A. Passi, D. Nikitovic, G.N. Tzanakakis, Receptor for hyaluronic acid-mediated motility (RHAMM) regulated HT1080 fibrosarcoma cell proliferation via a  $\beta$ -catenin/c-myc signaling axis, *Biochim. Biophys. Acta Gen. Subj.* 1860 (2016) 814–824.
- [7] H. Iwata, Pharmacologic and clinical aspects of intraarticular injection of hyaluronate, *Clin. Orthop. Relat. Res.* (289) (1993), 285–291.
- [8] R. Moseley, R.J. Waddington, G. Embery, Hyaluronan and its potential role in periodontal healing, *Dent. Update* 29 (2002) 144–148.
- [9] W.Y.J. Chen, G. Abatangelo, Functions of hyaluronan in wound repair, *Wound Rep. J.* (1999) 79–89.
- [10] A. Bogovic, J. Nizetic, N. Galic, D. Zeljezic, V. Micek, M. Mladinic, The effects of hyaluronic acid, calcium hydroxide, and dentin adhesive on rat odontoblast and fibroblasts, *Arh. Hig. Rada Toksikol.* 62 (2011) 155–161.
- [11] G. Sharon, A.B. Jason, S.F. Lino, A.T. Seth, L. Robert, V.N. Gordana, Hyaluronic acid hydrogel for controlled self-renewal and differentiation of human embryonic stem cells, *Proc. Natl. Acad. Sci. U. S. A.* 104 (2007) 11298–11303.
- [12] A. Moreno, A. Martinez, S. Olmedillas, S. Bello, F. de Miguel, Hyaluronic acid effect on adipose-derived stem cells, biological in vitro evaluation, *Rev. Esp. Cir. Ortop. Traumatol.* 59 (2015) 215–221.
- [13] R.M. Liu, R.G. Sun, L.T. Zhang, Q.F. Zhang, D.X. Chen, J.J. Zhong, J.H. Xiao, Hyaluronic acid enhances proliferation of human amniotic mesenchymal stem cells through activation of Wnt/ $\beta$ -catenin signaling pathway, *Exp. Cell Res.* 345 (2016) 218–229.
- [14] N. Sahiner, S.B. Sengel, Various amine functionalized halloysite nanotube as efficient metal free catalysts for  $\text{H}_2$  generation from sodium borohydride methanolysis, *Appl. Clay Sci.* 146 (2017) 517–525.
- [15] A.C. Santos, C. Ferreira, F. Veiga, A.J. Ribeiro, A. Panchal, Y. Lvov, A. Agarwal, Halloysite clay nanotubes for life sciences applications: from drug encapsulation to bioscaffold, *Adv. Colloid Interf. Sci.* 257 (2018) 58–70.

- [16] V. Pavlišnáková, Z. Fohlerová, D. Pavlišák, V. Khunová, L. Vojtová, Effect of halloysite nanotube structure on physical, chemical, structural and biological properties of elastic polycaprolactone/gelatin nanofibers for wound healing applications, *Mater. Sci. Eng. C* 91 (2018) 94–102.
- [17] J. Kurczewska, M. Ceglowski, B. Messyasz, G. Schroeder, Dendrimer-functionalized halloysite nanotubes for effective drug delivery, *Appl. Clay Sci.* 153 (2018) 134–143.
- [18] M. Liu, R. He, J. Yang, Z. Long, B. Huang, Y. Liu, C. Zhou, Polysaccharide-halloysite nanotube composites for biomedical applications: a review, *Clay Miner.* 51 (2016) 457–467.
- [19] H.A. Afshar, A. Ghaee, Preparation of aminated chitosan/alginate scaffold containing halloysite nanotubes with improved cell attachment, *Carbohydr. Polym.* 151 (2016) 1120–1131.
- [20] M. Liu, Y. Zhang, C. Wu, S. Xiong, C. Zhou, Chitosan/halloysite nanotubes bionanocomposites: structure, mechanical properties and biocompatibility, *Int. J. Biol. Macromol.* 51 (2012) 566–575.
- [21] E.A. Naumenko, I.D. Guryanov, R. Yendluri, Y.M. Lvov, R.F. Fakhruilin, Clay nanotube–biopolymer composite scaffolds for tissue engineering, *Nanoscale* 8 (2016) 7257–7271.
- [22] S.B. Sengel, M. Sahiner, N. Aktas, N. Sahiner, Halloysite-carboxymethyl cellulose cryogel composite from natural sources, *Appl. Clay Sci.* 140 (2017) 66–74.
- [23] S. Demirci, S.S. Suner, M. Sahiner, N. Sahiner, Superporous hyaluronic acid cryogel composites embedding synthetic polyethyleneimine microgels and Halloysite nanotubes as natural clay, *Eur. Polym. J.* 93 (2017) 775–784.
- [24] M. Liu, Z. Jia, D. Jia, C. Zhou, Recent advance in research on halloysite nanotubes-polymer nanocomposite, *Prog. Polym. Sci.* 39 (2014) 1498–1525.
- [25] V.I. Lozinsky, I.Y. Galaev, F.M. Plieva, I.N. Savina, H. Jungvid, B. Mattiasson, Polymeric cryogels as promising materials of biotechnological interest, *Trends Biotechnol.* 21 (2003) 445–451.
- [26] K. Bloch, A. Vanichkin, L.G. Damshkaln, V.I. Lovinsky, P. Vardi, Vascularization of wide pore agarose-gelatin cryogel scaffolds implanted subcutaneously in diabetic and non-diabetic mice, *Acta Biomater.* 6 (2010) 1200–1205.
- [27] B. Yetiskin, O. Okay, High-strength and self-recoverable silk fibroin cryogels with anisotropic swelling and mechanical properties, *Int. J. Biol. Macromol.* 122 (2019) 1279–1289.
- [28] N. Sahiner, S. Sagbas, M. Sahiner, C. Silan, P(TA) macro-, micro-, nanoparticle-embedded super porous p(HEMA) cryogels as wound dressing material, *Mater. Sci. Eng. C* 70 (2017) 317–326.
- [29] B. Yetiskin, C. Akinci, O. Okay, Cryogelation within cryogels: silk fibroin scaffolds with single-, double- and triple-network structures, *Polymer* 128 (2017) 47–56.
- [30] R. Li, G. Wu, Y. Ye, In vitro hemocompatibility of sulfonated polypropylene non-woven fabric prepared via a facile  $\gamma$ -ray pre-irradiation grafting method, *Appl. Surf. Sci.* 356 (2015) 1221–1228.
- [31] R.F. Fakhruilin, Y.M. Lvov, Halloysite clay nanotubes for tissue engineering, *Nanomedicine* 11 (2016) 2243–2246.
- [32] T. Shutava, R. Fakhruilin, Y. Lvov, Spherical and tubule nanocarriers for sustained drug release, *Curr. Opin. Pharmacol.* 18 (2014) 141–148.
- [33] S. Del Buffa, M. Bonini, F. Ridi, M. Severi, P. Losi, S. Volpi, T.A. Kayal, G. Soldani, P. Baglioni, Design and characterization of a composite material based on Sr(II)-loaded clay nanotubes included within a biopolymer matrix, *J. Colloid Interface Sci.* 448 (2015) 501–507.
- [34] M.V. Beridge, A.S. Tan, Characterization of the cellular reduction of 3-(4,5-dimethylthiazol-2-yl)-2,5-diphenyltetrazolium bromide (MTT): subcellular localization, substrate dependence, and involvement of mitochondrial electron transport in MTT reduction, *Arch. Biochem. Biophys.* 303 (1993) 474–482.
- [35] Y. Lvov, W. Wang, L. Zhang, R. Fakhruilin, Halloysite clay nanotubes for loading and sustained release of functional compounds, *Adv. Mater.* 28 (2016) 1227–1250.
- [36] M. Kryuchkova, A. Danilushkina, Y. Lvov, R. Fakhruilin, Evaluation of toxicity of nanoclays and graphene oxide in vivo: a *Paramecium caudatum* study, *Environ. Sci.: Nano* 3 (2016) 442–452.